

Qualitative and quantitative analysis of stability and instability dynamics of positive lattice solitons

Y. Sivan,¹ B. Ilan,² and G. Fibich³

¹*Department of Physics and Astronomy, Tel Aviv University, Tel Aviv 69978, Israel*

²*School of Natural Sciences, University of California, Merced, P.O. Box 2039, Merced, California 95344, USA*

³*Department of Applied Mathematics, Tel Aviv University, Tel Aviv 69978, Israel*

We present a unified approach for qualitative and quantitative analysis of stability and instability dynamics of positive bright solitons in multi-dimensional focusing nonlinear media with a potential (lattice), which can be periodic, periodic with defects, quasiperiodic, single waveguide, etc. We show that when the soliton is unstable, the type of instability dynamic that develops depends on which of two stability conditions is violated. Specifically, violation of the slope condition leads to an amplitude instability, whereas violation of the spectral condition leads to a drift instability. We also present a quantitative approach that allows to predict the stability and instability strength.

PACS numbers: 42.65 Jx, 42.65 Tg, 03.75 Lm

I. INTRODUCTION

Solitons, or solitary waves, are localized nonlinear waves that maintain their shape during propagation. They are prevalent in many branches of physics, and their properties have provided deep insight into complex nonlinear systems. The stability properties of solitons are of fundamental importance, in part because stable solitons are easier to observe in experiment and are usually the preferred choice in applications.

The first studies considered stability of solitons in homogeneous media. In recent years there has been a considerable interest in the study of solitons in lattice-type systems. Such solitons have been observed in optics using waveguide arrays, photo-refractive materials, photonic crystal fibers, etc., in both one-dimensional and multidimensional lattices, mostly periodic sinusoidal square lattices [1, 2, 3, 4, 5, 6, 7, 8, 9] or single waveguide potentials [10, 11], but also in discontinuous lattices (surface solitons) [12], radially-symmetric Bessel lattices [13], lattices with triangular or hexagonal symmetry [14, 15], lattices with defects [16, 17, 18, 19, 20, 21, 22], with quasicrystal structures [16, 23, 24, 25, 26, 27, 28] or with random potentials [29, 30]. Solitons have also been observed in the context of Bose-Einstein Condensates (BEC) [31, 32], where lattices have been induced using a variety of techniques.

Stability of lattice solitons has been studied in hundreds of papers. The majority of these papers focused on one specific physical configuration, i.e., a specific dimension (mostly in 1D), nonlinearity and lattice type. In addition, in several studies, general conditions for stability and instability were derived (see Section III). In all of these studies, the key question was whether the soliton is stable (yes) or unstable (no).

In a series of papers, Fibich, Sivan and co-workers [33, 34, 35, 36, 37] moved beyond this “yes/no approach” and developed a *qualitative* and *quantitative* approach to stability of positive lattice solitons. Specifically, they showed that the qualitative nature of the instability dynamics is determined by the stability condition which is being violated. In addition, they presented a quantitative approach that allows to predict the stability or instability strength. These papers considered the cases of a one-dimensional nonlinear lattice [33], a two-

dimensional nonlinear lattice [34], a one-dimensional linear delta-function potential [36] and narrow solitons in a linear lattice [35].

In this study, the results of [33, 34, 35, 36, 37] are combined into a unified theory for stability and instability of lattice solitons that can be summarized in a few rules (Section VI). We illustrate how these rules can be applied in a variety of examples that may be useful to experimental studies.

II. MODEL, NOTATION AND DEFINITIONS

In this manuscript, we study the stability and instability dynamics of lattice solitons of the nonlinear Schrödinger (NLS) equation with an external potential, which in dimensionless form is given by

$$iA_z(\vec{x}, z) + \Delta A + (1 - V_{nl}(\vec{x})) F(|A|^2) A - V_l(\vec{x}) A = 0. \quad (1)$$

This equation underlies many models of nonlinear wave propagation in nonlinear optics and in BEC. For example, in the context of laser beam propagation, $A(\vec{x}, z)$ corresponds to the electric field amplitude, z is the direction of propagation, $\vec{x} = (x_1, \dots, x_d)$ is the transverse d -dimensional space [e.g., the (x, y) plane for propagating in bulk medium] and $\Delta = \partial_{x_1 x_1} + \dots + \partial_{x_d x_d}$ is the d -dimensional diffraction term. The nonlinear term models the intensity-dependence of the refractive index. For example, $F(|A|^2) = |A|^2$ corresponds to the optical Kerr effect and $F(|A|^2) = 1/(1 + |A|^2)$ corresponds to photorefractive materials. The potentials V_l and V_{nl} correspond to a modulation of the linear and nonlinear refractive indices, respectively. In BEC, $z = t$ is time, $A(\vec{x}, t)$ represents the wave function of the mean-field atomic condensate, $F(|A|^2) = |A|^2$ represents contact (cubic) interaction, and the potentials V_l and V_{nl} are induced by externally applied electro-magnetic fields [38].

We denote by *soliton* any solution of Eq. (1) of the form $A(\vec{x}, z) = u(\vec{x})e^{-i\mu z}$, where μ is the propagation constant and $u(\vec{x})$, the soliton profile, is a real-valued function that decays to zero at infinity and satisfies

$$\Delta u + (1 - V_{nl}(\vec{x})) F(u^2)u + \mu u - V_l u = 0. \quad (2)$$

Solitons can exist only in the gaps of the linear problem

$$\Delta u + \mu u - V_l u = 0, \quad (3)$$

i.e., for values of μ such that the linear problem (3) does not have any non-trivial solution, see e.g., [39].

In this paper, we only consider positive solitons ($u > 0$). This is the generic case in the semi-infinite gap, i.e., when $-\infty < \mu < \mu_{BE}^{(V)}$, where $\mu_{BE}^{(V)}$ is the smallest eigenvalue of Eq. (3), at which the first band begins. Other gaps may exist for periodic lattices and the solitons in them are usually referred to as gap solitons. However, gap solitons are typically not positive and are therefore not covered by the theory presented in this paper.

We study solitons with a finite H_1 norm, where the H_1 norm is defined as $\|f\|_{H_1}^2 := \int (|f|^2 + |\nabla f|^2) d\vec{x}$. The standard notion of soliton stability in NLS theory is that of orbital stability. For Eq. (1) it is defined as follows:

Definition II.1 Let $u(\vec{x})$ be a solution of Eq. (2) with propagation constant μ . Then, $u(\vec{x})e^{-i\mu z}$ is an orbitally stable solution of the NLS (15) if for all ε , exists $\delta(\varepsilon) > 0$ such that for any initial condition A_0 such that $\inf_{\gamma \in \mathbb{R}} \|A_0 - u e^{i\gamma}\|_{H_1} < \delta$, the corresponding solution A of Eq. (15) satisfies

$$\sup_{z \geq 0} \inf_{\gamma \in \mathbb{R}} \|A(\vec{x}, z) - u(\vec{x})e^{i\gamma}\|_{H_1} < \varepsilon.$$

III. SOLITON STABILITY – HISTORICAL OVERVIEW

The first analytic result on soliton stability was obtained by Vakhitov and Kolokolov [40]. Based on a linear stability analysis, they showed that a necessary condition for soliton stability is that

$$\frac{dP}{d\mu} < 0, \quad P(\mu) := \int |u|^2 d\vec{x}, \quad (4)$$

i.e., the soliton power decreases with increasing propagation constant μ . Subsequently, this result was derived from a rigorous nonlinear stability analysis [41, 42]. 7 Grillakis, Shatah and Strauss (GSS) analyzed stability of solitons of a general Hamiltonian system [43, 44]. In the case of positive solitons ($u > 0$), the GSS stability theory can be stated as follows. Let

$$d(\mu) = \mathcal{H} - \mu \mathcal{P} \\ = \int [|\nabla u|^2 + (V_l(\vec{x}) - \mu) u^2 - (1 - V_{nl}(\vec{x})) G(u)] d\vec{x},$$

where $G = \int_0^u F(u'^2) du'$, let $p(d'') = 1$ if $d''(\mu) < 0$ and $p(d'') = 0$ if $d''(\mu) > 0$, and let $n_-(L_+)$ be the number of negative eigenvalues of the linearized operator

$$L_+ = -\Delta - \mu - (1 - V_{nl}(\vec{x})) (F(u^2) - 2u^2 F') + V_l. \quad (5)$$

Then, $A = u e^{-i\mu z}$ is orbitally stable if $n_-(L_+) = p(d'')$, and orbitally unstable if $n_-(L_+) - p(d'')$ is odd [43, 44].

In order to avoid confusion, we point out that the value of μ in L_+ is fixed, so that the eigenvalues and eigenfunctions of L_+ are the solutions of

$$L_+(\mu; V) f(\vec{x}) = \lambda(\mu; V) f(\vec{x}).$$

In this paper, we rely on the following Stability Theorem:

Theorem III.1 Let $u(\vec{x})$ be a positive solution of Eq. (2) with propagation constant μ . Then, $A = u(\vec{x})e^{-i\mu z}$ is an orbitally-stable solution of the NLS (1) if both of the following conditions hold:

1. The **slope (Vakhitov-Kolokolov) condition**

$$\frac{dP}{d\mu} < 0, \quad P(\mu) := \int |u|^2 d\vec{x}. \quad (6)$$

2. The **spectral condition**:

$$n_-(L_+) = 1, \quad (7)$$

i.e., L_+ has exactly one negative eigenvalue of multiplicity one.

Theorem III.1 was proved for nonlinear potentials [33] and for linear potentials which are bounded and decay to zero at infinity [45, 46], and in the narrow soliton (semi-classical) limit in the subcritical case [47]. The proof can be extended to the case of potentials bounded from below (i.e., not necessarily periodic or decaying to zero) [48].

Theorem III.1 is an extension of the classical stability theory of GSS [43, 44]. Indeed, since $d'(\mu) = P(\mu)$, the sign of d'' is the same as the sign of the power slope. Hence, in the GSS theory, stability and instability depend on a *combination* of the slope condition (6) and the spectral condition as follows: If both the slope condition and the spectral condition are satisfied, the soliton is stable, whereas if either the slope condition is satisfied and $n_-(L_+)$ is even, or if the slope condition is violated and $n_-(L_+)$ is odd, the soliton is unstable. There are two cases not covered by the GSS theory: When the slope condition is satisfied and $n_-(L_+)$ is odd, and when the slope condition is violated and $n_-(L_+)$ is even [72]. Theorem III.1 shows that in these two cases, the solitons are unstable. Hence, Theorem III.1 implies that *there is a “decoupling” of the slope and spectral conditions, in the sense that both are needed for stability, and violation of either of them would lead to instability.*

A. Review of stability conditions in homogeneous media

Stability and instability of solitons in *homogeneous* media (i.e., $V \equiv 0$) have been extensively investigated [49]. In this case, $\mu_{BE}^{(V \equiv 0)} = 0$, i.e., the semi-infinite gap associated with Eq. (3) is $(-\infty, 0)$. For every $\mu < 0$ and $\vec{x}_0 \in \mathbb{R}^d$, there exists a soliton centered at \vec{x}_0 which is radially-symmetric in $r = |\vec{x} - \vec{x}_0|$, positive, and monotonically decaying in r .

In the case of a power-law nonlinearity $F(|u|) = |u|^{2\sigma}$, the slope condition (6) depends on the dimension d and nonlinearity exponent σ as follows [50]:

1. In the subcritical case $d < 2/\sigma$, $\frac{dP}{d\mu} < 0$. Hence, the slope condition is satisfied.
2. In the critical case $d = 2/\sigma$, the soliton power does not depend on μ , i.e., $\frac{dP}{d\mu} \equiv 0$. Hence, the slope condition is violated.
3. In the supercritical case $d > 2/\sigma$, $\frac{dP}{d\mu} > 0$. Hence, the slope condition is violated.

Thus, the slope condition is satisfied only in the subcritical case.

When $V \equiv 0$, the spectrum of L_+ is comprised of three parts [50], see Figure 1:

1. A simple negative eigenvalue $\lambda_{\min} < 0$, with a corresponding positive and radially-symmetric eigenfunction $f_{\min} = u^{\sigma+1}$ [35].
2. A zero eigenvalue with multiplicity d , i.e., $\lambda_{0,j}^{(V)} = 0$ with eigenfunctions $f_j = \frac{\partial u}{\partial x_j}$ for $j = 1, \dots, d$. These zero eigenvalues manifest the translation invariance in a homogeneous medium in all d directions.
3. A strictly positive continuous spectrum $[-\mu, \infty)$.

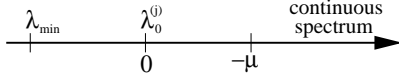


FIG. 1: (Color online) The spectrum of L_+ in a homogeneous medium.

In a homogeneous medium the bound states are also translation invariant and orbital stability is defined modulo the phase and translation invariance. As such, the spectral condition is satisfied and therefore stability is determined by the slope condition alone. Hence, solitons in a homogeneous medium with a power-law nonlinearity are stable only in the subcritical case.

B. Stability conditions in inhomogeneous media

Below we investigate how the two stability conditions are affected by a potential/lattice.

Generically, in the subcritical ($d < 2/\sigma$) and supercritical ($d > 2/\sigma$) cases, the slope has an $\mathcal{O}(1)$ magnitude in a homogeneous medium. Hence, a weak lattice can affect the magnitude of the slope but not its sign, see e.g., [35]. Clearly, a sufficiently strong lattice can alter the sign of the slope, see e.g. [36] for the subcritical case and [51, 52] for the supercritical case. The situation is very different in the critical case ($d = 2/\sigma$). Indeed, since the slope is zero in a homogeneous medium, any potential, no matter how weak, can affect the sign of the slope.

The potential can affect the spectrum of L_+ in two different ways: 1) shift the eigenvalues, and 2) open gaps (bounded-intervals) in the continuous spectrum, see Figure 2. In general, the minimal eigenvalue of L_+ remains negative, i.e.,

$\lambda_{\min}^{(V)} < 0$, the continuous spectrum remains positive, and the zero eigenvalues can move either to the right or to the left. Hence, generically, the spectrum of L_+ has the following structure:

1. A simple negative eigenvalue $\lambda_{\min}^{(V)} < 0$ with a positive eigenfunction $f_{\min}^{(V)} > 0$.
2. Perturbed-zero eigenvalues $\lambda_{0,j}^{(V)}$ with eigenfunctions $f_j^{(V)}$, for $j = 1, \dots, d$.
3. A positive continuous spectrum, sometimes with a band-gap structure, beginning at $-\mu_{BE}^{(V)} > 0$.

This structure of the spectrum was proved in [33] for solitons in the presence of a *nonlinear lattice*, i.e., Eq. (15) with $V_l \equiv 0$. For a *linear lattice*, the proof of the negativity of $\lambda_{\min}^{(V)}$ is the same as in [33]. The proof of the positivity of $-\mu_{BE}^{(V)}$ is the same as in [33] for potentials that decay to 0 as $|\vec{x}| \rightarrow \infty$.

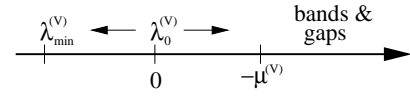


FIG. 2: (Color online) The spectrum of L_+ in an inhomogeneous medium.

Since $\lambda_{\min}^{(V)} < 0$ and the continuous spectrum is positive, the spectral condition (7) reduces to

$$\lambda_{0,j}^{(V)} \geq 0, \quad j = 1, \dots, d, \quad (8)$$

i.e., that all the perturbed-zero eigenvalues are non-negative. Generically, the equivalent spectral condition (8) is satisfied when the soliton is centered at a local minimum of the potential, but violated when the soliton is centered at a local maximum or saddle point of the potential [33, 34, 35, 36, 37, 47, 53, 54, 55].

We note that in many previous studies, only the slope condition was checked for stability. As Theorem III.1 shows, however, “ignoring” the spectral condition is justified only for solitons centered at lattice minima, since only then the spectral condition is satisfied. In all other cases, checking only the slope condition usually lead to incorrect conclusions regarding stability.

C. Instability and collapse

We recall that in a homogeneous medium with a power nonlinearity, all solutions of the subcritical NLS exist globally, while the critical and supercritical NLS admits collapsing (singular) solutions [56]. Hence, in a homogeneous medium, the two phenomena of collapse and of soliton instability appear together. In fact, the two phenomena are directly related, since in the critical and supercritical cases, the instability of the solitons is manifested by the fact that they can collapse under infinitesimally small perturbations (i.e., a *strong instability*).

As we shall see below, the situation is different in inhomogeneous media. Indeed, the soliton can be unstable even if all solutions of the corresponding NLS exist globally. Conversely, the soliton can be stable, yet undergo collapse under a sufficiently strong perturbation. Such results on the “decoupling” of instability and collapse have already appeared in [16, 33, 34, 35, 36, 57]. In all of these cases, the “decoupling” is related to the absence of translation invariance.

IV. QUALITATIVE APPROACH – CLASSIFICATION OF INSTABILITY DYNAMICS

The dynamics of orbitally-stable solitons is relatively straightforward - the solution remains close to the unperturbed soliton. On the other hand, there are several possible ways for a soliton to become unstable: it can undergo collapse, complete diffraction, drift, breakup into separate structures, etc.

Theorem III.1 is our starting point for the classification of the instability dynamics, since it suggests that there are two independent mechanisms for (in)stability. In fact, we show below that the instability dynamics depends on which of the two conditions for stability is violated.

As noted in Section III C, in a homogeneous medium with a power-law nonlinearity, when the slope condition is violated, the soliton can collapse (become singular) under an infinitesimal perturbation. In this case, the soliton amplitude becomes infinite as its width shrinks to zero. If the perturbation is in the “opposite direction”, the soliton diffracts to zero, i.e., its amplitude goes to zero as its width becomes infinite. More generally, in other types of nonlinearities or in the presence of inhomogeneities, there are cases where the slope condition is violated but collapse is not possible (e.g., in the one-dimensional NLS with a saturable nonlinearity [58]). In such cases, a violation of the slope condition leads to an amplitude instability whereby infinitesimal changes of the soliton can result in large changes of the beam amplitude, but not in collapse or total diffraction. Accordingly, we refer to the instability which is related to the violation of the slope condition as an *amplitude instability* (rather than as a collapse instability).

When the soliton is unstable because the spectral condition is violated, it undergoes a *drift instability* whereby infinitesimal shifts of the initial soliton location lead to a lateral movement of the soliton away from its initial location. The mathematical explanation for the drift instability is as follows. The spectral condition is associated with the perturbed-zero eigenvalue $\lambda_{0,j}^{(V)}$ and the corresponding eigenmode f_j . In the homogeneous case, the eigenmodes $f_j = \frac{\partial u}{\partial x_j}$ are odd. By continuity from the homogeneous case, the perturbed-zero eigenmodes $f_j^{(V)}$ in the presence of a potential are also odd. When the spectral condition is violated, these odd eigenmodes grow, resulting in an *asymmetric* distortion of the soliton, which gives rise to a drift of the beam away from its initial location, see also Section V. The mathematical relation between the violation of the spectral condition and the drift instability is further developed in Section V.

The drift dynamics also has an intuitive physical explanation.

According to Fermat’s Principle, light bends towards regions of higher refractive-index. Positive values of the potential V correspond to negative values of the refractive index, hence, Fermat’s principle implies that beams bend towards regions of lower potential. Moreover, since generically, the spectral condition is satisfied for solitons centered at a lattice minimum but violated for solitons centered at a lattice maximum, one sees that the drift instability of solitons centered at lattice maxima and the drift stability of solitons centered at lattice minima is a manifestation of Fermat’s principle.

V. QUANTITATIVE APPROACH

As noted, the soliton is drift-unstable when $\lambda_{0,j}^{(V)} < 0$ but drift-stable when $\lambda_{0,j}^{(V)} \geq 0$. Thus, there is a discontinuity in the behavior as $\lambda_{0,j}^{(V)}$ passes through zero. Nevertheless, one can expect the transition between drift instability and drift stability to be continuous, in the sense that as $\lambda_{0,j}^{(V)}$ approaches zero from below, the rate of the drift becomes slower and slower. Similarly, we can expect that as $\lambda_{0,j}^{(V)}$ becomes more negative, the drift rate will increase.

The quantitative relation between the value of $\lambda_{0,j}^{(V)}$ and the drift rate was found *analytically* in [35] for *narrow* solitons in a Kerr medium with a linear lattice and later in [37] for solitons of any width, for a general nonlinearity and for any potential. Let us define the center of mass of a perturbed soliton in the x_j coordinate as

$$\langle x_j \rangle := \frac{1}{P} \int x_j |A|^2 d\vec{x}. \quad (9)$$

Then, the dynamics of $\langle x_j \rangle$ is initially governed by the linear oscillator equation

$$\frac{d^2}{dz^2} \langle x_j \rangle = \Omega_j^2 (\langle x_j \rangle - x_{0,j}), \quad (10)$$

with the initial conditions

$$\begin{cases} \langle x_j \rangle_{z=0} = \int x_j |A_0|^2 d\vec{x} / P, \\ \frac{d}{dz} \langle x_j \rangle_{z=0} = 2d \cdot \text{Im} \int A_0^* \nabla A_0 d\vec{x} / P. \end{cases} \quad (11)$$

Here, $x_{0,j}$ is the location of the lattice extremum in the j th direction (not to be confused with $\langle x_j \rangle_{z=0}$, the value of the center of mass at $z = 0$). The forcing is given by

$$\Omega_j^2 = -C_j \lambda_{0,j}^{(V)}, \quad C_j = \frac{(f_{0,j}^{(V)}, f_{0,j}^{(V)})}{(L_-^{-1} f_{0,j}^{(V)}, f_{0,j}^{(V)})}, \quad (12)$$

where $f_{0,j}^{(V)}$ is the eigenmode of L_+ that corresponds to $\lambda_{0,j}^{(V)}$, i.e., the eigenmode along the x_j direction, the operator L_- is given by

$$L_- = -\Delta - \mu - (1 - V_{nl}(\vec{x})) F(u^2) + V_l,$$

and the inner product is defined as $(f, g) = \int f g^* d\vec{x}$.

Since L_- is non-negative for positive solitons, it follows that $C_j > 0$. Therefore, when $\lambda_{0,j}^{(V)}$ is negative, Ω_j is real and when $\lambda_{0,j}^{(V)}$ is positive, Ω_j is purely imaginary. Hence, by Eqs. (10)-(12), it follows that the lateral dynamics of a general incident beam centered near a lattice minimum is

$$\langle x_j \rangle = \langle x_j \rangle_{z=0} \cos(|\Omega_j|z) + \frac{d}{dz} \langle x_j \rangle_{z=0} \sin(|\Omega_j|z), \quad (13)$$

i.e., the soliton drifts along the x_j coordinate at the rate Ω_j . On the other hand, the lateral dynamics of a general incident beam centered near a lattice maximum is

$$\langle x_j \rangle = \langle x_j \rangle_{z=0} \cosh(\Omega_j z) + \frac{d}{dz} \langle x_j \rangle_{z=0} \sinh(\Omega_j z). \quad (14)$$

i.e., the soliton is pulled back towards $x_{0,j}$ by a restoring force which is proportional to Ω_j^2 , so that it undergoes oscillations around $x_{0,j}$ in the x_j coordinate with the period $|\Omega_j|$.

As noted, the soliton is amplitude-unstable when the slope $dP/d\mu$ is non-negative, and amplitude-stable when the slope is negative. In a similar manner to the continuous transition between drift stability and instability, one can expect the transition between amplitude stability and instability to be continuous. In other words, one can expect the magnitude of the slope to be related to the strength of amplitude stability or instability. At present, the quantitative relation between the magnitude of the slope and the strength of the stability is not known, i.e., we do not have a relation such as (10). However, numerical evidence for this link was found in several of our earlier studies [33, 34, 35, 36]. For example, in the case of amplitude-stable solitons that collapse under sufficiently large perturbations, it was observed that as the magnitude of the slope increases, the magnitude of the perturbation that is needed for the soliton to collapse also increases. Thus, the magnitude of the slope is related to the size of the basin of stability [33, 34, 35]. In cases of amplitude-stable solitons where collapse is not possible, when the magnitude of the slope increases, the amplitude stability is stronger in the sense that for a given perturbation, the maximal deviation of the soliton from its initial amplitude decreases [36].

A. Physical vs. Mathematical stability

The quantitative approach is especially important in the limiting cases of weak stability/instability. For example, consider a soliton for which the two conditions for stability are met, but for which $\lambda_{0,j}^{(V)}$ or the slope are very small in magnitude. Such a soliton is orbitally stable, yet it can become unstable under perturbations which are quite small compared with typical perturbations that exist in experimental setups. Hence, such a soliton is “mathematically stable” but “physically unstable”, see e.g., [33]. Conversely, consider an unstable soliton for which either $\lambda_{0,j}^{(V)}$ is negative but very small in magnitude or the slope is positive but small. In this case, the instability develops so slowly so that it can be sometimes neglected over the propagation distances of the exper-

iment. Such a soliton is therefore “mathematically unstable” but “physically stable” [35].

VI. GENERAL RULES

We can summarize the results described so far by several general rules for stability and instability of bright positive lattice solitons.

The *qualitative approach* rules of the are:

- QL1 Bright positive lattice solitons of NLS equations can become unstable in *only* two ways: Amplitude-instability or drift-instability.
- QL2 Violation of the slope condition leads to an amplitude-instability, i.e., either initial diffraction or initial self-focusing. In the latter case, self-focusing can lead to collapse, but not always.
- QL3 The spectral condition is generically satisfied when the soliton is centered at a potential minimum and violated when the soliton is centered at a potential maximum or saddle point.
- QL4 Violation of the spectral condition leads to a drift-instability, i.e., an initial lateral drift of the soliton from the potential maximum/saddle point towards a nearby lattice minimum.

The *quantitative theory* rules are:

- QN1 The strength of the amplitude- and drift- stability and instability depends on the magnitude of the slope $\left| \frac{dP}{d\mu} \right|$ and the magnitude of $|\lambda_{0,j}^{(V)}|$, respectively.
- QN2 The lateral dynamics of the beam is initially given by Eqs. (10)-(12).

The above rules were previously demonstrated for 1D solitons in a periodic nonlinear lattice [33], for an anisotropic 2D lattice [34] and for several specific cases of linear lattices [35, 36]. In this paper, we demonstrate that these rules apply in a *general setting* of dimension, nonlinearity, linear/nonlinear lattice with any structure and for any soliton width. In particular, we use these general rules to explain the dynamics of lattice solitons in a variety of examples that were not studied before.

VII. NUMERICAL METHODOLOGY

Below we present a series of numerical computations that illustrate the qualitative and quantitative approaches presented in Sections IV-V. We present results for the 2D cubic NLS

$$iA_z(x, y, z) + \Delta A + |A|^2 A - V(x, y)A = 0, \quad (15)$$

with periodic lattices, lattices with a vacancy defect, and lattices with a quasicrystal structure. There are two reasons for

the choice of the 2D cubic NLS. First, this equation enables us to illustrate the instability dynamics in dimensions larger than one, in particular, in cases where the dynamics in each direction is different (e.g., as for solitons centered at saddle points). Second, the 2D cubic NLS enables us to elucidate the distinction between instability and collapse. Indeed, we recall that a necessary condition for collapse in the 2D cubic NLS is that the power of the beam exceeds the critical power $P_c \approx 11.7$.

We first compute the soliton profile by solving Eq. (2) using the spectral renormalization method [59]. Once the solitons are computed for a range of values of μ , the slope condition (6) is straightforward to check. In order to check the spectral condition (7), the perturbed-zero eigenvalues $\lambda_{0,j}^{(V)}$ (and the corresponding eigenfunctions f_j) of the discrete approximation of the operator L_+ are computed using the numerical method presented in [35, Appendix D]. The value of Ω_j is calculated from Eq. (12) by inversion of the discrete approximation of the operator L_- .

Eq. (15) is solved using an explicit Runge-Kutta four-order finite-difference scheme. Following [33, 34, 35, 36], the initial conditions are taken to be the unperturbed lattice soliton $u(x, y)$ with *either*

1. a small *power perturbation*, i.e.,

$$A_0(x, y) = \sqrt{1 + c} u(x, y), \quad (16)$$

where c is a small constant that expresses the excess power of the input beam above that of the unperturbed soliton, *or*

2. a small *lateral shift*, i.e.,

$$A_0(x, y) = u(x - \Delta x_0, y - \Delta y_0), \quad (17)$$

where Δx_0 and Δy_0 are small compared with the characteristic length-scale (e.g., period) of the potential.

The motivation for this choice of perturbations is that each perturbation predominantly excites only one type of instability. Indeed, by Eq. (10)-(11), it is easy to verify that under a power perturbation, the center of mass will remain at its initial location (cf. [33, 34, 36]), i.e., no lateral drift will occur. In this case, only an amplitude instability is possible. On the other hand, the asymmetric perturbation (17) will predominantly excite a drift instability (but if the soliton is drift-stable, this perturbation can excite an amplitude instability, see Figure 6).

The advantage of the perturbations (16)-(17) over adding random noise to the input soliton is that they allow us to control the type of instability that is excited. Moreover, grid convergence tests are also simpler. Once the NLS solution is computed, it is checked for amplitude and drift instabilities by monitoring the evolution of the normalized peak intensity

$$I(z) := \frac{\max_{x,y} |A(x, y, z)|^2}{|A_0(x, y)|^2}, \quad (18)$$

and of the center of mass (9), respectively.

By definition II.1 of stability, any perturbation to an unstable soliton will ultimately drive it away from the unperturbed soliton. However, as the magnitude of the perturbation is reduced, by continuity from the unperturbed case, the distance at which the instability manifests itself will become longer. Therefore, for a numerical test done over a finite propagation distance, it is impossible to “prove” numerically that the solution is unstable under infinitesimally small perturbations. Hence, *numerically, the difference between an orbitally stable and unstable soliton is only quantitative*: For a given perturbation, the deviation from the soliton is significantly larger for an unstable soliton compared with a stable soliton.

In particular, from Eqs. (10)-(11) it follows that for a spectrally *stable* soliton, 1) the maximal deviation of the center of mass decreases linearly with the lateral shift and 2) the period of the oscillations is independent of the initial shift. On the other hand, for a spectrally *unstable* soliton, the deviation of the center of mass grows exponentially with the propagation distance at a rate Ω , and its maximal value depends on the lattice details rather than on the magnitude of the initial lateral shift. In particular, the maximal deviation is not linearly dependent on the magnitude of the initial lateral shift as in the stable case. In addition, as the magnitude of the lateral shift becomes smaller, the propagation distance at which the deviation of the center of mass becomes significant, increases, again, unlike the stable case. Although we have no similar analytic prediction of the amplitude dynamics under a power perturbation, we note that similar observations were made for the amplitude dynamics, i.e., 1) for a given perturbation, the deviation of the amplitude from the soliton amplitude is significantly larger for an unstable soliton compared with a stable soliton and its maximal value depends on the lattice details rather than on the magnitude of the initial perturbation, 2) as the magnitude of the initial perturbation becomes smaller, the amplitude changes accumulate more slowly, (see e.g., [36]).

VIII. PERIODIC SQUARE LATTICES

We first choose the sinusoidal square lattice

$$V(x, y) = \frac{V_0}{2} [\cos^2(2\pi x) + \cos^2(2\pi y)], \quad (19)$$

which is depicted in Figure 3. We consider this to be the simplest 2D periodic potential, as all the local extrema are also global extrema. This lattice can be created through interference of two pairs of counter-propagating plane waves, and is standard in experimental setups, see, e.g., [60, 61]. The stability and instability dynamics are investigated below for solitons centered at the lattice maxima, minima, and saddle points, see Figure 3(b).

A. Solitons at lattice minima

We first investigate solitons centered at the lattice minimum $(x_0, y_0) = (0.25, 0.25)$. Figure 4(a) shows that the power of

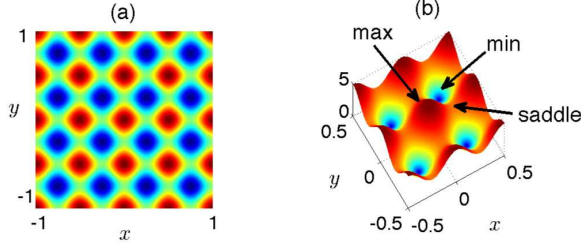


FIG. 3: (Color online) The sinusoidal square lattice given by Eq. (19) with $V_0 = 5$. (a) Top view. (b) Side view. Red and blue correspond to lattice maxima and minima, respectively. The solitons investigated below are centered at the lattice maximum (0,0), lattice minimum (0.25,0.25), and saddle point (0.25,0).

solitons at lattice minima is below the critical power for collapse, i.e., $P(\mu) < P_c \approx 11.7$ for all μ . As the soliton becomes narrower ($\mu \rightarrow -\infty$), the soliton power approaches P_c from below (as was shown numerically in [39] for this lattice and analytically in [35] for any linear lattice). In addition, as the soliton becomes wider ($\mu \rightarrow \mu_{BE}^{(V)}$, the edge of the first band), its power approaches P_c from below (rather than becomes infinite, as implied in [39]). The minimal power is obtained at $\mu = \mu_m \cong -10$. The power curve thus has a stable branch for narrow solitons ($-\infty < \mu < \mu_m$) where the slope condition is satisfied, and an unstable branch for wide solitons ($\mu_m < \mu < \mu_{BE}^{(V)}$) where the slope condition is violated. Therefore, wide solitons should be amplitude-unstable while narrow solitons should be amplitude-stable. Figure 4(b) shows that, as expected for solitons at lattice minima, $\lambda_0^{(1)} = \lambda_0^{(2)} > 0$ for all μ . Hence, the spectral condition is fulfilled. Consequently, solitons at lattice minima should not experience a drift instability.

In order to excite the amplitude instability alone, we add to the soliton a small power perturbation, see Eq. (16). Since the difference between a stable and unstable soliton can be numerically observed only quantitatively (see Section VII), we choose two solitons with the same power ($P \cong 0.98P_c$), from the stable branch ($\mu = -31$) and from the unstable branch ($\mu = -3$), and apply to them the same power perturbations ($c = 0.5\%, 1\%, 2\%$).

When $c = 0.5\%$ and 1% , the input power is below the threshold for collapse ($P < P_c$). In these cases, the self-focusing process is arrested and, during further propagation, the normalized peak intensity undergoes oscillations (see Figures 5(a) and (b)). For a given perturbation, the oscillations are significantly smaller for the stable soliton compared with the unstable soliton.

When $c = 2.5\%$, the input power is above the threshold for collapse ($P > P_c$) and the solutions undergo collapse. Therefore, for such large perturbations, collapse occurs for both stable and unstable solitons, i.e., even when *both the slope and spectral conditions are fulfilled*. This shows yet again that in an inhomogeneous medium, collapse and instability are not necessarily related.

In order to confirm that solitons centered at a lattice minimum do not undergo a drift instability, we shift the soli-

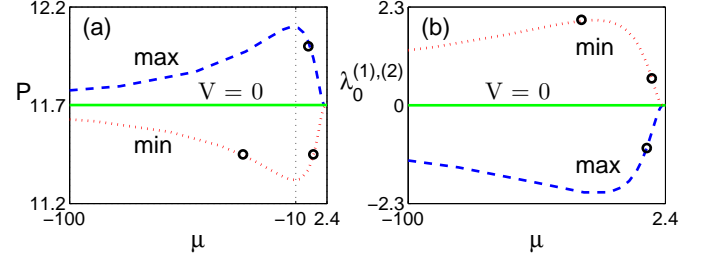


FIG. 4: (Color online) (a) Power, and (b) perturbed-zero eigenvalues, as functions of the propagation constant, for solitons centered at a maximum (blue, dashes) and minimum (red, dots) of the lattice (19) with $V_0 = 5$. Also shown are the corresponding lines for the homogeneous NLS equation (solid, green). The circles (black) correspond to the values used in Figs. 5-8.

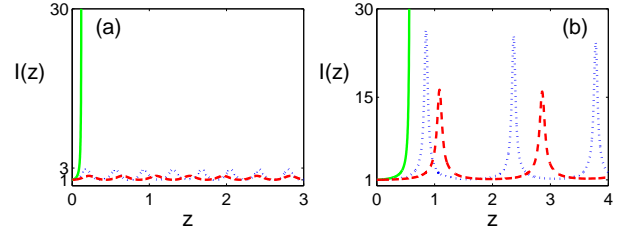


FIG. 5: (Color online) Normalized peak intensity (18) of solutions of Eq. (15) with the periodic lattice (19) with $V_0 = 5$. Initial conditions are power-perturbed solitons [see Eq. (16)] centered at a lattice minimum: (a) Soliton from the stable branch ($\mu = -31$); (b) Soliton from the unstable branch ($\mu = -3$). Input powers are 0.5% (red dots), 1% (blue dashes), and 2.5% (solid green) above the soliton power.

ton slightly upward by using the initial condition (17) with $(\Delta x_0, \Delta y_0) = (0, 0.04)$. Under this perturbation, the solution of Eq. (10) is

$$\langle x \rangle \equiv 0, \quad \langle y \rangle = \Delta y_0 \cdot \cos(|\Omega_y|z). \quad (20)$$

In addition, by Eq. (12), $\Omega_y \approx 11.12i$ for $\mu = -31$ and $\Omega_y \approx 2.58i$ for $\mu = -3$. Figure 6(a1) shows that for $\mu = -31$, the center of mass in the y -direction of the position-shifted soliton follows the theoretical prediction (20) accurately over several oscillations. In addition, the center of mass in the x -direction remain at $x = 0$ (data not shown), in agreement with Eq. (20). Thus, the soliton is indeed drift-stable.

The situation is more complex for $\mu = -3$. In this case, the position-shifted soliton follows the theoretical prediction (20) over more than 2 diffraction lengths (i.e., for $z > z_0$ where $z_0 \approx 1$), but then deviates from it, see Figure 6(b1). The reason for this instability is that for $\mu = -3$, the slope condition is violated. Since the position-shifted initial condition can also be viewed as an asymmetric amplitude perturbation $\Delta A = u(x - \Delta x_0, y - \Delta y_0) - u(x, y)$, an amplitude instability is excited and the soliton amplitude decreases (as its width increases), see Figure 6(b2). Obviously, once the soliton amplitude changes significantly, the theoretical prediction for the lateral dynamics is no longer valid. In order to be convinced

that the initial instability in this case is of an amplitude-type rather than drift-type, we note that for $\mu = -31$ for which the slope condition is satisfied, the soliton remains amplitude-stable, see Figure 6(a2).

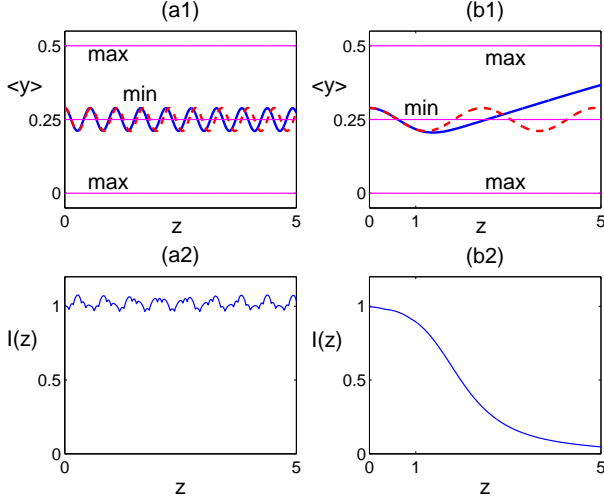


FIG. 6: (Color online) Dynamics of solutions of Eq. (15) with the periodic lattice (19) with $V_0 = 5$. Initial conditions are position-shifted solitons [see Eq. (17)] centered at a lattice minimum, with $(\Delta x_0, \Delta y_0) = (0, 0.04)$. (a1) and (a2) show the center of mass $\langle y \rangle$ and normalized peak intensity (18) for $\mu = -31$; (b1) and (b2) are the same as (a1) and (a2) but for $\mu = -3$.

B. Solitons at lattice maxima

We now investigate solitons centered at the lattice maximum $(x_0, y_0) = (0, 0)$. Figure 4 shows that solitons at lattice maxima have the opposite stability characteristics compared with those of solitons centered at lattice minima: The slope condition is violated for narrow solitons and satisfied for wide solitons, the power is above P_c for all μ , and the perturbed-zero eigenvalues $\lambda_{0,j}^{(V)}$ are always negative. Interestingly, for the specific choice of the lattice (19), the powers and perturbed-zero eigenvalues at lattice maxima and minima are approximately, but not exactly, images of each other with respect to the case of a homogeneous medium.

The negativity of the perturbed-zero eigenvalues implies that solitons centered at a lattice maximum undergo a drift instability (see Figure 8(b)). However, if the initial condition is subject to a power perturbation, see Eq. (16), then no drift occurs. In this case, stability is determined by the slope condition. For example, Figure 7 shows the dynamics of a power-perturbed wide soliton for which the slope condition is satisfied. When the soliton's input power is increased by 0.5%, the solution undergoes small focusing-defocusing oscillations, as in Figure 5(a), i.e., it is stable under symmetric perturbations. When the soliton's input power is increased by 1%, the perturbation exceeds the “basin of stability” of the soliton [35] and the soliton undergoes collapse. These results

again demonstrate that collapse and instability are independent phenomena.

If the initial condition is asymmetric with respect to the lattice maximum, the soliton will undergo a drift instability. In Figure 8 we excite this instability with a small upward shift, namely, Eq. (17) with $(\Delta x_0, \Delta y_0) = (0, 0.02)$. Under this perturbation, the solution of Eq. (10) is

$$\langle x \rangle \equiv 0, \quad \langle y \rangle = \Delta y_0 \cdot \cosh(\Omega_y z). \quad (21)$$

with $\Omega_y \approx 3.9$. In the initial stage of the propagation ($z < 0.5$) the soliton drifts toward the lattice minimum – precisely following the asymptotic prediction (20), see Figure 8(b), but the soliton's amplitude is almost constant, see Figure 8(a). During the second stage of the propagation ($0.5 < z < 0.99$) the soliton drifts somewhat beyond the lattice minimum as it begins to undergo self-focusing. In the final stage ($0.99 < z < 1$) the soliton undergoes collapse (Figure 8(a)). The *global dynamics* can be understood in terms of the stability conditions for solitons centered at lattice minima and maxima as follows. The initial soliton, which is centered at a lattice maximum, satisfies the slope condition but violates the spectral condition. Consistent with these traits, the soliton is amplitude-stable but undergoes a drift instability. As the soliton gets closer to the lattice minimum, it can be viewed as a perturbed soliton centered at the lattice minimum, for which the spectral condition is fulfilled and the soliton power is below P_c (see Figure 4(b)). Indeed, at this stage, the drift is arrested because the beam is being attracted back towards the lattice minimum. Moreover, the beam now is a strongly power-perturbed soliton, since the beam power ($\approx 1.03P_c$) is $\approx 6\%$ above the power of the soliton at a lattice minimum. Hence, in a similar manner to the results of Figure 5(a), the perturbation exceeds the “basin of stability” and the soliton undergoes collapse.

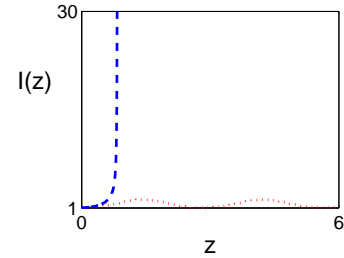


FIG. 7: (Color online) Same as Figure 5(a) for a soliton at a lattice maximum with $\mu = -5$ (stable branch) and input power that is 0.5% (red dots) and 1% (blue dashes) above the soliton power.

C. Solitons at a saddle point

From the didactic point of view, it is interesting also to consider solitons centered at a saddle point since they exhibit a combination of the features of solitons at lattice minima and maxima. To show this, we compute solitons centered at the saddle point $(x_0, y_0) = (0.25, 0)$ of the lattice (19).

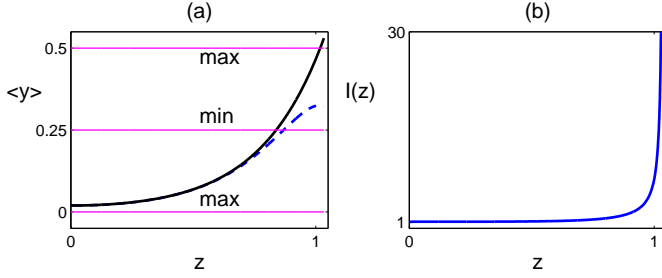


FIG. 8: (Color online) Dynamics of a soliton at a lattice maximum with $\mu = -5$, which is position-shifted according to (17) with $(\Delta x_0, \Delta y_0) \approx (0, 0.02)$. (a) Center of mass in the y coordinate (blue, dashes) and the analytical prediction (Eq. (21) with $\Omega_y \approx 3.9$, solid black). Location of lattice minimum and maxima are denoted by thin magenta and black horizontal lines, respectively. (b) Normalized peak intensity.

Figure 9(a) shows that the zero eigenvalues bifurcate into $\lambda_0^{(1)} > 0$ on the stable x manifold, i.e., along direction in which the saddle is a minimum, and to $\lambda_0^{(2)} < 0$ on the unstable y manifold, where the saddle is a maximum.

The opposite signs of the perturbed-zero eigenvalues imply a different dynamics in each of these directions. In order to excite only the drift instability, we solve Eq. (15) with $\mu = -12$ which belongs to the amplitude-stable branch (see Figure 9(b2)). For this value of μ , the perturbed zero eigenvalues are $\lambda_0^{(1)} \approx 1.7$ and $\lambda_0^{(2)} \approx -1.8$. By (12), the theoretical prediction for the oscillation period is $\Omega_x \approx |7i| = 7$ whereas the drift rate is $\Omega_y \approx 7.2$. Hence, the theoretical prediction for the dynamics of the center of mass is

$$\langle x \rangle \approx 0.25 + \Delta x_0 \cdot \cos(7z), \quad \langle y \rangle \approx \Delta y_0 \cdot \cosh(7.2z).$$

Indeed, a shift in the x direction $(\Delta x_0, \Delta y_0) \approx (0.0156, 0)$ leads to oscillation in the x -direction (Figure 10(a)) while $\langle y \rangle$ (Figure 10(b)) and the amplitude (Figure 10(c)) are unchanged. On the other hand, a shift in the y direction $(\Delta x_0, \Delta y_0) \approx (0, 0.0156)$ leads to a drift instability in the y -direction (Figure 10(b)) but has no effect on $\langle x \rangle$ (Figure 10(a)). In both the stable and unstable directions, the center of mass follows the analytical prediction remarkably well. Figure 10(c) also shows that once the soliton drifts beyond the lattice minimum, the beam undergoes collapse. This can be understood using the same reasoning used for solitons that drift from a lattice maximum (see explanation for Figure 8 in Section VIII B).

We also note that for the specific choice of the lattice (19), the values of the perturbed-zero eigenvalues on the stable and unstable manifolds are nearly indistinguishable from those of the perturbed-zero eigenvalues that correspond to solitons centered at a lattice minimum and maximum, respectively. This can be understood by rewriting the lattice (19) as

$$V(x, y) = \frac{V_0}{2} [1 - \cos^2(2\pi(x - 0.25)) + \cos^2(2\pi y)]. \quad (22)$$

Thus, apart from the constant part (i.e., the first term), the

difference between the lattices is the sign before the x -component of the lattice. In that sense, in the x direction, the saddle point is *equivalent* to a maximum point, hence, the similarity between the eigenvalues. Another consequence of the $x - y$ symmetry of the lattice (19) is that the soliton has approximately the critical power P_c for all μ , i.e., $P(\mu) \approx P_c$, which is approximately the average of the powers of solitons at maxima and minima (see Figure 9(b1,b2)). As noted before, this will be no longer true if the lattice changes in the x and y directions will no longer be equal.

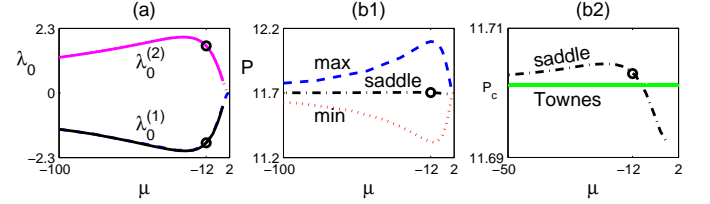


FIG. 9: (Color online) (a) The perturbed-zero eigenvalues at the saddle point. One eigenvalue is shifted to positive values (magenta), and is indistinguishable from the eigenvalue at lattice minima (red); one eigenvalue is shifted to negative values (black), and is indistinguishable from the eigenvalue at lattice maxima (blue). (b1) Same data as in Figure 4(a), with the addition of data for solitons centered at a saddle point of the lattice (black, dash-dots). (b2) same as (b1) showing only the data for solitons centered at a saddle point (black, dash-dots) and for the homogeneous medium soliton (green line).

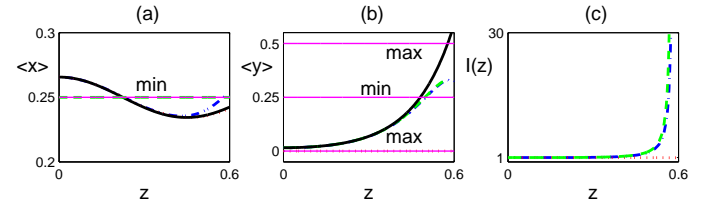


FIG. 10: (Color online) Dynamics of a soliton centered at a saddle point $(x_0, y_0) = (0.25, 0)$ of the lattice (19) with $\mu = -12$ and shifts along: (i) the stable x direction $[(\Delta x_0, \Delta y_0) \approx (0.0156, 0)]$, red dots, (ii) the unstable y direction $[(\Delta x_0, \Delta y_0) \approx (0, 0.0156)]$, green dashes, (iii) the diagonal direction $[(\Delta x_0, \Delta y_0) \approx (0.0156, 0.0156)]$, blue, dash-dots. (a) Center of mass $\langle x \rangle$. (b) Center of mass $\langle y \rangle$. (c) Normalized peak intensity.

If we apply perturbations in the stable and unstable directions simultaneously $(\Delta x_0, \Delta y_0) \approx (0.0156, 0.0156)$, the dynamics in each coordinate is nearly identical to the dynamics when the perturbation was applied just in that direction. Thus, there is a “decoupling” between the (lateral dynamics in the) x and y directions. Indeed, this decoupling follows directly from Eq. (10).

D. Solitons at a shallow-maximum

We now consider solitons of the periodic potential

$$V(x, y) = \frac{V_0}{25} [2 \cos(2\pi x) + 2 \cos(2\pi y) + 1]^2, \quad (23)$$

where $V_0 = 5$ and the normalization by 25 implies that $V_0 = \max_{x,y} V(x, y)$. Unlike the lattice (19), the lattice (23) also has shallow local maxima that are not global maxima [e.g., at (0.5, 0.5)].

The stability and instability dynamics of solitons centered at global minima, maxima and saddle points of the lattice are similar to the case of the lattice (19), which was already studied. Hence, we focus only on the stability of solitons centered at a shallow maximum.

Since the lattice is invariant under a 90° rotation, the perturbed-zero eigenvalues are equal, i.e., $\lambda_0^{(1)} = \lambda_0^{(2)}$. However, unlike solitons centered at a global maximum, the corresponding perturbed-zero eigenvalues are negative only for small values of μ (narrow beams) but become positive for large values of μ (wide beams), see Figure 12(b). The reason for the positivity of $\lambda_0^{(1)} = \lambda_0^{(2)}$ despite being centered at a lattice maximum is as follows. For narrow solitons, the region where the “bulk of the beam” is located is of higher values of the potential compared with the immediate surrounding, hence, the solitons “feel” an effective lattice maximum. On the other hand, for wider solitons, the “bulk of the beam” is centered mostly at the shallow lattice maximum and the surrounding lower potential regions. Hence, although the very center of the soliton is at the shallow lattice maximum, these solitons are effectively centered at the lattice minimum with respect to the nearest global lattice maxima (see also [33], Section 4.5). The transition of the qualitative stability properties between narrow and wide solitons described above occurs when the soliton’s width is on the order of the lattice period. Similarly, a comparison of Figure 12(a) and Figure 4(a) shows that the $P(\mu)$ reflects the transition between properties which are characteristic to solitons centered at lattice maxima and minima. Indeed, for narrow solitons ($\mu \rightarrow -\infty$) is similar to the power of solitons centered at a global maximum, i.e., the power is above critical and the slope is positive. On the other hand, $P(\mu)$ curve for wide solitons ($\mu \rightarrow \mu_{BE}^{(V)}$) is similar to the power of solitons centered at a (simple) lattice minimum, i.e., the power is below critical and the slope is positive too.

Numerical simulations (Figure 13) demonstrate this transition. For a narrow soliton ($\mu = -12$), the theoretical prediction for the dynamics of the center of mass is $\langle x \rangle \cong 0.5 + \Delta x_0 \cosh(4.14z)$ and $\langle y \rangle \cong 0.5 + \Delta y_0 \cosh(4.14z)$. Indeed, the narrow soliton drifts away from the shallow maximum toward the nearby (global) lattice minimum (Figure 13(a1)) and then undergoes collapse (Figure 13(a2)). This dynamics is similar to that of solitons centered near lattice maximum or a saddle of a the lattice (19), see Sections VIII B and VIII C. On the other hand, for the wide soliton ($\mu = -2$), the theoretical prediction for the dynamics of the center of mass is $\langle x \rangle \cong 0.5 + \Delta x_0 \cos(1.6z)$ and $\langle y \rangle \cong 0.5 + \Delta y_0 \cos(1.6z)$. Indeed, this soliton remains stable, undergoing small position

oscillations around the shallow maximum (Figure 13(b)). This dynamics is the same as for solitons centered at a minimum of the lattice (19), see Figure 6(a). As in previous examples, the numerical results are in excellent agreement with the analytic prediction (10)-(12).

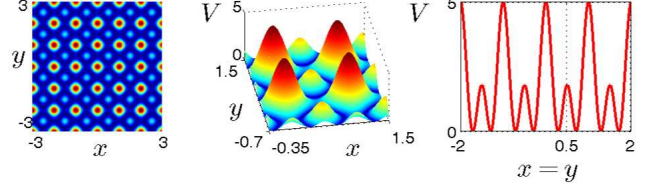


FIG. 11: (Color online) The shallow maximum periodic lattice given by Eq. (23) with $V_0 = 5$. (a) Top view. (b) Side view. (c) Cross section along the line $x = y$.

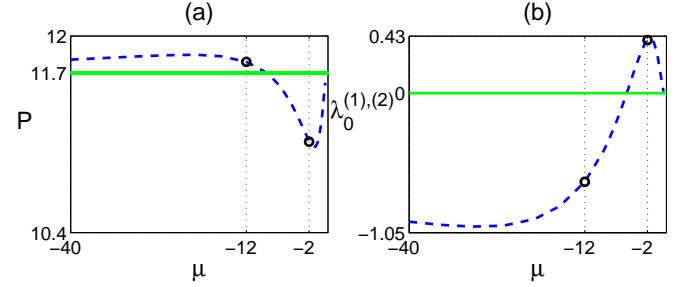


FIG. 12: (Color online) Same as Figure 4 for solitons centered at a shallow local maximum of the shallow-maximum periodic lattice (23).

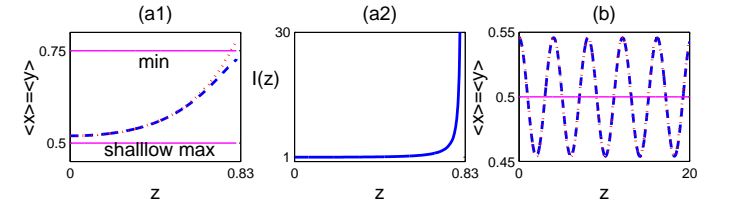


FIG. 13: (Color online) Dynamics of a perturbed soliton at shallow-maximum periodic lattice (23) with a narrow soliton [(a1) and (a2) with $\mu = -12$] and a wide soliton [(b) with $\mu = -2$], and using $(\Delta x_0, \Delta y_0) = (0.05, 0.05)$. (a1) Center of mass $\langle x \rangle = \langle y \rangle$ of the narrow soliton (blue, dashes) and the analytical prediction (red dots). (a2) Normalized peak intensity of the narrow soliton. (b) Same as (a1) for the wide soliton.

IX. PERIODIC LATTICES WITH DEFECTS

Defects are unavoidable in natural or artificial materials. Solitons in periodic lattices with defects have drawn much attention both experimentally and theoretically, see e.g., [16, 62, 63] to name a few. The complexity of the lattice details offers

an opportunity to demonstrate the relative ease of applying the stability/dynamics criteria to predict and decipher the soliton dynamics in them. As an example, we study lattices with a point defect. Our analysis can also extend to different types of defects such as line defects, see e.g. [16].

We consider the lattice (23)

$$V(x, y) = \frac{V_0}{25} \left| 2 \cos(2\pi x) + 2 \cos(2\pi y) + e^{i\theta(x, y)} \right|^2, \quad (24)$$

where the phase function $\theta(x, y)$ is given by

$$\theta(x, y) = \tan^{-1} \left(\frac{y - y_0}{x} \right) - \tan^{-1} \left(\frac{y + y_0}{x} \right), \quad (25)$$

see Figure 14 and also [16]. Compared with the shallow-maximum periodic lattice (23), here the constant (DC) component (the third term in the lattice) attains a phase distortion which creates an (effective) vacancy defect at $(0, 0)$, which is a shallow-maximum. Further, far away from the origin, the potential (24) is locally similar to the shallow-maximum periodic lattice (23). This is a generic example of a *point* defect, as opposed to a *line* defect [64]. In what follows, we consider solitons centered at the vacancy defect $(x_0, y_0) = (0, 0)$.

The stability properties of solitons in the shallow-maximum periodic (23) and vacancy-defect (24) lattices are strikingly similar, as can be seen from Figs. 12 and 15. In both cases, there is a marked transition between narrow and wide solitons and this transition occurs when the soliton width is of the order of the lattice period. Indeed, numerical simulations show that the dynamics of perturbed solitons is qualitatively similar in both cases – compare Figures 13 and 16. We do note that unlike the shallow-maximum periodic lattice, the perturbed-zero eigenvalues of the vacancy lattice bifurcate into different, though similar, values. The reason for this is the phase function (25) is not invariant by 90° rotations.

Inspecting the lattice surfaces (Figures 11 and 14), it is clearly seen that the reason for the similarity between the shallow-maximum periodic and vacancy lattices is that the vacant site is essentially a shallow local maximum itself – and only a bit shallower than those of the shallow-maximum periodic lattice (see Figure 14).

In Figure 17 we give a detailed graphical illustration of a typical instability dynamics due to a violation of the spectral condition. Figure 17(a)-(c) show contours of the soliton profiles superposed on the contour plot of the lattice. It can be seen that as a result of the initial position shift, the soliton drifts towards the lattice minimum and that it self-focuses at the same time. Figure 17(d) shows the trajectory of the beam across the lattice. In addition, Figure 17(e) shows the center of mass dynamics as a function of the intensity $I(z)$. This shows that initially, the perturbed soliton undergoes a drift instability with little self-focusing, but that once the collapse accelerates, it is so fast so that the drift dynamics becomes negligible.

X. QUASICRYSTAL LATTICES

Next, we investigate solitons in quasicrystal lattices. Such lattices appear naturally in certain molecules [65, 66], have

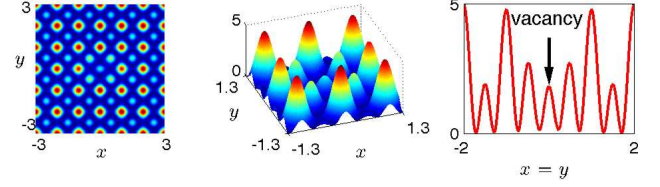


FIG. 14: (Color online) Same as Figure 11 for solitons centered at the “vacancy” of the lattice (24).

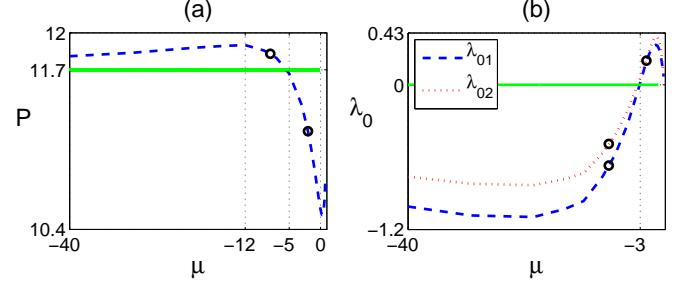


FIG. 15: (Color online) Same as Figure 4 for solitons at the vacancy of the lattice (24). (c) The perturbed-zero eigenvalues $\lambda_0^{(1),(2)}$ are slightly different from each other. The circles (black) correspond to the values used in Figure 16.

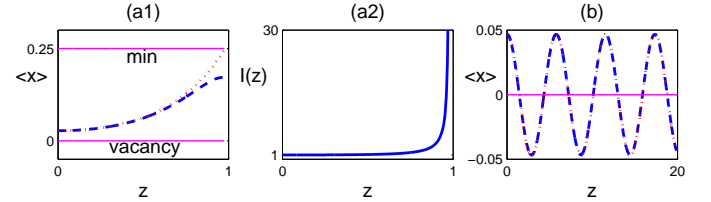


FIG. 16: (Color online) Same as Figure 13 but for the vacancy lattice (24). Here $\Omega_x \approx 3$ in (a2) and $\Omega_x \approx 1.09i$ in (b). In both cases the $\langle y \rangle$ dynamics (not shown) is similar (but not identical) to the $\langle x \rangle$ dynamics.

been investigated in optics [16, 23, 24, 25, 26] and in BEC [67], and can be formed optically by the far-field diffraction pattern of a mask with point-apertures that are located on the N vertices of a regular polygon, or equivalently, by the sum of N plane waves (cf. [16, 68]) with wavevectors (k_x, k_y) equally distributed over the unit circle. The corresponding potential is given by

$$V(x, y) = \frac{V_0}{N^2} \left| \sum_{n=0}^{N-1} e^{i(k_x^{(n)} x + k_y^{(n)} y)} \right|^2, \quad (26)$$

where $(k_x^{(n)}, k_y^{(n)}) = (K \cos(2\pi n/N), K \sin(2\pi n/N))$ [73]. The normalization by N^2 implies that $V_0 = \max_{x,y} V(x, y)$. The potential (26) with $N = 2, 3, 4, 6$ yields periodic lattices. All other values of N correspond to quasicrystals, which have a local symmetry around the origin and long-range order, but, unlike periodic crystals, are not invariant under spatial trans-

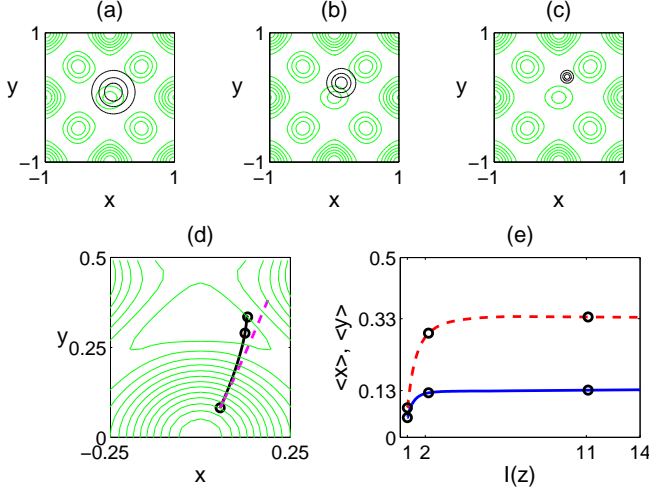


FIG. 17: (Color online) (a)–(c): contours of the intensity $|u(x, y, z)|^2$ (blue) superimposed on the vacancy lattice (green) with initial conditions corresponding to the mode with $\mu = -8$ that is initially shifted in the (x, y) plane to $(\Delta x_0, \Delta y_0) = (0.05, 0.1)$, i.e., at an angle of 63° to the y axis. (a) $z = 0$, $I \approx 1$, (b) $z = 0.51$, $I \approx 2.18$, (c) $z = 0.63$, $I \approx 11.1$. (d) Center of mass dynamics (black curve) and the analytical prediction (magenta, dashes) superimposed on the contours of the potential (green). (e) $\langle x \rangle$ (blue, solid) and $\langle y \rangle$ (red, dashes) as functions of $I(z)$. Circles (black) correspond to the z -slices shown in (a)–(c).

lation [69].

We first consider the case $N = 5$ (a Penrose quasicrystal) for solitons centered at the lattice maximum $(x_0, y_0) = (0, 0)$, see Figure 18. Since the soliton profile and stability are affected mostly by the lattice landscape near its center, we can expect the stability properties of the Penrose lattice soliton at $(0, 0)$ to be qualitatively the same as for a soliton at a lattice maximum of a periodic lattice. Indeed, Figure 19 reveals the typical stability properties of solitons centered at a lattice maximum: An amplitude-unstable branch for narrow solitons, an amplitude-stable branch for wider solitons and negative perturbed zero-eigenvalues (compare e.g. with Figure 8). Therefore, the Penrose soliton will drift from the lattice maximum under asymmetric perturbations and if the soliton is sufficiently narrow, it can also undergo collapse.

Figure 19 presents also the data for a perfectly periodic lattice ($N = 4$) and for a higher-order quasicrystal ($N = 11$). One can see that the stability properties in these lattices is qualitatively similar to the $N = 5$ case. The only marked difference as N increases is that the soliton's power becomes larger for a given μ .

These results show that in contrast to the significant effect of the quasi-periodicity on the dynamics of linear waves (compared with the effect of perfect periodicity [24]), the effect of quasi-periodicity on the dynamics of solitons is small.

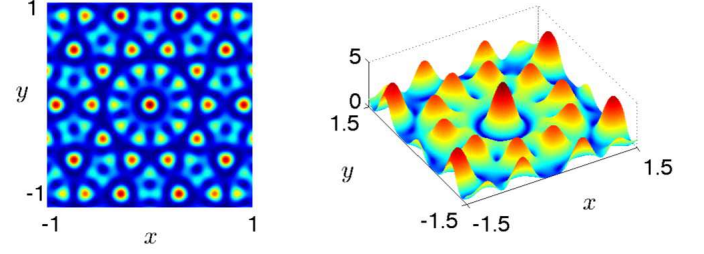


FIG. 18: (Color online) Same as Figure 11(a)+(b) for the Penrose quasicrystal lattice given by Eq. (26) with $N = 5$ and $V_0 = 5$.

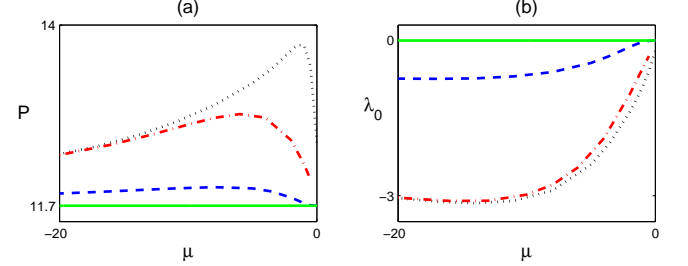


FIG. 19: (Color online) Same as Figure 4 for solitons at the maxima of the lattices (26) with $N = 4$ (periodic lattice, dashed blue line), $N = 5$ (Penrose quasicrystal lattice, dash-dotted red line), $N = 11$ (higher-order quasicrystal lattice, dotted black line), and the homogeneous NLS soliton (solid green line).

XI. SINGLE WAVEGUIDE POTENTIALS

So far we have studied potentials which are either periodic, almost periodic or quasiperiodic, i.e., they extend in all space. However, our theory applies also to localized potentials, e.g., single or multiple waveguide potentials, for which the potential decays to zero at infinity. For such potentials, there are two possible limits where either the soliton is wider or narrower than the width of the potential. In the former limit, the potential can be approximated as a point defect in an homogeneous medium. Then, the dynamics is governed by

$$iA_z(\vec{x}, z) + \Delta A + |A|^{2\sigma} A - \gamma \delta(\vec{x}) A = 0, \quad (27)$$

where γ is a real constant. This case was studied in [36] for one transverse dimension $\vec{x} = x$. In the latter limit, only the local variation of the potential affects the soliton profile and stability, hence, the potential can be expanded as

$$V(x) = V(0) + \frac{1}{2}V''(0)x^2 + \dots$$

This case was studied in [35]. In both of these studies, the profiles, power slope and perturbed-zero eigenvalues can be computed exactly or asymptotically. It was proved that the perturbed-zero eigenvalues are negative for solitons centered at lattice maxima (repulsive potential) and are positive for solitons centered at lattice minima (attractive potential). Hence, in the latter case, stability is determined by the slope

condition. In those two studies, detailed numerical simulations were presented. Hence, we do not repeat these results here.

XII. FINAL REMARKS

In this paper, we presented a unified approach for analyzing the stability and instability dynamics of positive bright solitons. This approach consists of a *qualitative* characterization of the type of instability, and a *quantitative* estimation of the instability rate and the strength of stability. This approach was summarized by several rules (Section VI) and applied to a variety of numerical examples (Sections VIII-X), thus revealing the similarity between a variety of physical configurations which, *a priori*, look very different from each other. In that sense, our approach differs from most previous studies which considered a specific physical configuration.

One aspect which was emphasized in the numerical examples is the excellent agreement between direct numerical simulations of the NLS and the reduced equations for the lateral dynamics, Eqs. (10)-(12). We note that different reduced equations for the lateral dynamics were previously derived under the assumption that the beam remains close to the initial soliton profile (see e.g. [70]) or by allowing the soliton parameters to vary along the propagation (see e.g., [71] and references therein). These approaches, as well as ours, are valid only as long as the beam profile remains close to a soliton profile. However, unlike these previous approaches, Eqs. (10)-(12) are based on the link between the linear stability theory

and the lateral dynamics. This link shows that in contrast to the ansatz used in previous works, the beam profile evolves as a soliton perturbed by the eigenfunction $f_{0,j}^{(V)}$. The validity of this perturbation analysis was manifested by the excellent fit between the reduced Eqs. (10)-(12) and the numerical simulations for a variety of lattice types. To the best of our knowledge, such an agreement was not achieved with the previous approaches.

The numerical examples in this paper were for two-dimensional Kerr media with various linear lattices. Together with our previous studies which were done for narrow solitons in any dimension [35], a linear delta-function potential [36] and for nonlinear lattices [33, 34], there is a strong numerical evidence that our qualitative and quantitative approaches apply to positive solitons in any dimension, any type of nonlinearity (e.g., saturable) as well as for other lattice configurations, e.g., “surface” or “corner” solitons [12].

As noted, our analysis shows that for positive bright solitons, only two types of instabilities are possible - amplitude instability or drift instability. Other types of instabilities such as modulational instability may appear, but only for non-positive solitons (e.g., gap solitons or vortex solitons). A formulation of a qualitative and quantitative theories for such solitons requires further study.

Acknowledgments

We acknowledge useful discussions with M.I. Weinstein and M.J. Ablowitz. The research of Y. Sivan and G. Fibich was partially supported by BSF grant no. 2006-262.

-
- [1] H. Eisenberg, Y. Silberberg, R. Morandotti, A. Boyd, and J. Aitchison, Phys. Rev. Lett. **81**, 3383 (1998).
 - [2] L. Carr, K. Mahmud, and W. Reinhardt, Phys. Rev. A **64**, 033603 (2001).
 - [3] N. Efremidis, D. Christodoulides, S. Sears, J. Fleischer, and M. Segev, Phys. Rev. E **66**, 046602 (2002).
 - [4] J. Fleischer, M. Segev, N. Efremidis, and D. Christodoulides, Nature **422**, 147 (2003).
 - [5] D. Christodoulides, F. Lederer, and Y. Silberberg, Nature **424**, 817 (2003).
 - [6] A. Sukhorukov, Y. Kivshar, H. Eisenberg, and Y. Silberberg, IEEE J. Quant. Elec. **39**, 31 (2003).
 - [7] N. Efremidis, J. Hudock, D. Christodoulides, J. Fleischer, O. Cohen, and M. Segev, Phys. Rev. Lett. **91**, 213906 (2003).
 - [8] D. Neshev, Y. Kivshar, H. Martin, and Z. Chen, Opt. Lett. **29**, 486 (2004).
 - [9] T. Pertsch, U. Peschel, J. Kobelke, K. Schuster, H. Bartelt, S. Nolte, A. Tünnermann, and F. Lederer, Phys. Rev. Lett. **93**, 053901 (2004).
 - [10] Y. Linzon, R. Morandotti, M. Volatier, V. Aimez, R. Ares, and S. Bar-Ad, Phys. Rev. Lett. **99**, 133901 (2007).
 - [11] H. Sakaguchi and M. Tamura, J. Phys. Soc. Jap. **73**, 503 (2004).
 - [12] K. Makris, S. Suntsov, D. Christodoulides, G. Stegeman, and A. Hache, Opt. Lett. **30**, 2466 (2005).
 - [13] Y. Kartashov, V. Vysloukh, and L. Torner, Phys. Rev. Lett. **93**, 093904 (2004).
 - [14] P. Kevrekidis, B. Malomed, and Y. Gaididei, Phys. Rev. E **66**, 016609 (2002).
 - [15] C. Rosberg, D. Neshev, A. Sukhorukov, W. Krolikowski, and Y. Kivshar, Opt. Lett. **32**, 397 (2007).
 - [16] M. Ablowitz, B. Ilan, E. Schonbrun, and R. Piestun, Phys. Rev. E - Rap. Comm. **74**, 035601 (2006).
 - [17] F. Fedele, J. Yang, and Z. Chen, Stud. Appl. Math. **115**, 279 (2005).
 - [18] I. Makasyuk and Z. Chen, Phys. Rev. Lett. **96**, 223903 (2006).
 - [19] H. Martin, E. Eugenieva, Z. Chen, and D. Christodoulides, Phys. Rev. Lett. **92**, 123902 (2004).
 - [20] M. Qi, E. Lidorikis, P. Rakich, S. Johnson, J. Joannopoulos, E. Ippen, and H. Smith, Nature **429**, 538 (2004).
 - [21] H. Y. Ryu, S. H. Kim, H. G. Park, and Y. H. Lee, J. Appl. Phys. **93**, 831 (2003).
 - [22] J. Yang and Z. Chen, Phys. Rev. E **73**, 026609 (2006).
 - [23] R. Bratfalean, A. Peacock, N. Broderick, K. Gallo, and R. Lewen, Opt. Lett. **30**, 424 (2005).
 - [24] B. Freedman, G. Bartal, M. Segev, R. Lifshitz, D. Christodoulides, and J. Fleischer, Nature **440**, 1166 (2006).
 - [25] R. Lifshitz, A. Arie, and A. Bahabad, Phys. Rev. Lett. **95**, 133901 (2005).
 - [26] W. Man, M. Megens, P. Steinhardt, and P. Chaikin, Nature **436**, 993 (2005).
 - [27] A. D. Villa, S. Enoch, G. Tayeb, V. Pierro, V. Galdi, and F. Capolino, Phys. Rev. Lett. **94**, 183903 (2005).
 - [28] P. Xie, Z.-Q. Zhang, and X. Zhang, Phys. Rev. E **67**, 026607

- (2003).
- [29] T. Schwartz, G. Bartal, S. Fishman, and M. Segev, *Nature* **446**, 52 (2007).
 - [30] Y. Lahini, A. Avidan, F. Pozzi, M. Sorel, R. Morandotti, D. Christodoulides, and Y. Silberberg, *Phys. Rev. Lett.* **100**, 013906 (2008).
 - [31] F. Abdullaev, A. Gammal, A. Kamchatnov, and L. Tomio, *Int. J. of Mod. Phys. B* **19**, 3415 (2005).
 - [32] V. Konotop, in *Dissipative Solitons ed. N. Akhmediev* (Springer, 2005).
 - [33] G. Fibich, Y. Sivan, and M. Weinstein, *Physica D* **217**, 31 (2006).
 - [34] Y. Sivan, G. Fibich, and M. Weinstein, *Phys. Rev. Lett.* **97**, 193902 (2006).
 - [35] Y. Sivan, G. Fibich, N. Efremidis, and S. Barad, *Nonlinearity* **21**, 509 (2008).
 - [36] S. Le-Coz, R. Fukuizumi, G. Fibich, B. Ksherim, and Y. Sivan, *Physica D* (To appear).
 - [37] Y. Sivan, G. Fibich, and B. Ilan, *Phys. Rev. E(R)* (2008).
 - [38] C. Pethick and H. Smith, *Bose-Einstein Condensation in Dilute Gases* (Cambridge University Press, 2001).
 - [39] Z. Musslimani and J. Yang, *J. Opt. Soc. Am. B* **21**, 973 (2004).
 - [40] M. Vakhitov and A. Kolokolov, *Radiophys. Quant. Elec.* **16**, 783 (1973).
 - [41] T. Cazenave and P.-L. Lions, *Comm. Math. Phys.* **85**, 549 (1982).
 - [42] M. Weinstein, *Comm. Pure Appl. Math.* **39**, 51 (1986).
 - [43] M. Grillakis, J. Shatah, and W. Strauss, *J. Funct. Anal.* **74**, 160 (1987).
 - [44] M. Grillakis, J. Shatah, and W. Strauss, *J. Funct. Anal.* **94**, 308 (1990).
 - [45] H. Rose and M. Weinstein, *Physica D* **30**, 207 (1988).
 - [46] M. Weinstein, *Contemporary Mathematics* **99**, 213 (1989).
 - [47] Y.-G. Oh, *Comm. Math. Phys.* **121**, 11 (1989).
 - [48] B. Ilan and M. Weinstein, Preprint.
 - [49] C. Sulem and P. L. Sulem, *The Nonlinear Schrödinger Equation* (Springer, 1999).
 - [50] M. Weinstein, *SIAM J. Math. Anal.* **16**, 472 (1985).
 - [51] D. Mihalache, D. Mazilu, F. Lederer, B. Malomed, L.-C. Crasovan, Y. Kartashov, and L. Torner, *Phys. Rev. A* **72**, 021601 (2005).
 - [52] D. Mihalache, D. Mazilu, F. Lederer, B. Malomed, L.-C. Crasovan, Y. Kartashov, and L. Torner, *Phys. Rev. E* **70**, 055603(R) (2004).
 - [53] D. Pelinovsky, A. Sukhorukov, and Y. Kivshar, *Phys. Rev. E* **70**, 036618 (2004).
 - [54] Z. Rapti, P. Kevrekidis, V. Konotop, and C. Jones, *J. Phys. A.* **40**, 14151 (2007).
 - [55] T. Lin and J. Wei, *SIAM J. Math. Anal.* (To appear).
 - [56] M. Weinstein, *Comm. Math. Phys.* **87**, 567 (1983).
 - [57] G. Fibich and F. Merle, *Physica D* **155**, 132 (2001).
 - [58] B. Gisin, R. Driben, and B. Malomed, *J. Opt. B* **6**, S259 (2004).
 - [59] M. Ablowitz and Z. Musslimani, *Opt. Lett.* **30**, 2140 (2005).
 - [60] M. Cristiani, O. Morsch, J. Müller, D. Ciampini, and E. Arimondo, *Phys. Rev. A* **65**, 063612 (2002).
 - [61] M. Jona-Lasinio, O. Morsch, M. Cristiani, N. Malossi, J. Müller, E. Courtade, M. Anderlini, and E. Arimondo, *Phys. Rev. Lett.* **91**, 230406 (2003).
 - [62] G. Alfimov, P. Kevrekidis, V. Konotop, and M. Salerno, *Phys. Rev. E* **66**, 046608 (2002).
 - [63] J. Wang, J. Yang, and Z. Chen, *Phys. Rev. A* **76**, 013828 (2007).
 - [64] T. Baba, *Nature Photonics* **1**, 11 (2007).
 - [65] D. Shechtman, I. Blech, D. Gratias, and J. W. Cahn, *Phys. Rev. Lett.* **53**, 1951 (1984).
 - [66] M. P. Marder, *Condensed Matter Physics* (Wiley-Interscience, 2001).
 - [67] L. Sanchez-Palencia and L. Santos, *Phys. Rev. A* **72**, 053607 (2005).
 - [68] J. Nye and M. Berry, *Proc. Royal Soc. London* **336**, 165 (1974).
 - [69] M. Senechal, *Quasicrystals and Geometry* (Cambridge University Press, 1995).
 - [70] Y. Kartashov, A. Zelenina, L. Torner, and V. Vysloukh, *Opt. Lett.* **29**, 766 (2004).
 - [71] Y. Kivshar and G. Agrawal, *Optical Solitons* (Academic Press, 2003).
 - [72] Note, however, that despite the coupling of the slope and spectral conditions, the slope condition is still a necessary condition in the GSS formalism.
 - [73] We note that Eq. (26) can also describe the lattices (23) and (24) for $N = 4$ and an additional $k = 0$ phase modulated plane wave.